



13th World Conference on Earthquake Engineering
Vancouver, B.C., Canada
August 1-6, 2004
Paper No. 3249

EVALUATING THE SEISMIC PERFORMANCE OF STONE CANYON DAM WITH 2-D AND 3-D ANALYSES

Wolfgang H. Roth¹, Ethan M. Dawson¹, Paul Somerville¹, Craig A. Davis², Clifford C. Plumb²

SUMMARY

The seismic performance of Stone Canyon dam, a 160-ft high earth embankment partially founded on liquefiable alluvium, was analyzed with 2-D and 3-D nonlinear effective-stress models using the explicit finite-difference program FLAC. For the 2-D analyses soil behavior was simulated with an elastic-plastic Mohr-Coulomb model fully coupled with a cyclic-stress based pore-pressure generation scheme. Shaking-induced permanent deformations and post-shaking safety factors were analyzed with both 2-D and 3-D models. A comparison of analysis results highlights the inherent conservatism of evaluating the seismic stability of short dams across narrow canyons with 2-D plane-strain models.

INTRODUCTION

Stone Canyon Dam is owned and operated by the Los Angeles Department of Water and Power. It is located on the south slope of the Santa Monica Mountains overlooking the posh Bel Air section of Los Angeles. A plan view and sections of the dam are presented in Figures 1 through 3. The embankment was originally constructed in the early 1920's of locally derived earth fill materials which were, for the most part, hydraulically placed on top of existing alluvium and bedrock. A few years after filling the reservoir, excessive seepage through the dam was observed, and after several unsuccessful attempts to control the



seepage through extensive grouting, the upstream portion of the dam was rebuilt in the mid 1950's. The new portion of the dam was constructed as a roller-compacted earth fill founded on bedrock, but the older downstream portion remained on alluvium. Construction was completed in 1956.

The investigation described in this paper was performed in 2002 in an effort to re-assess the dam's earthquake performance in light of new site-specific seismicity data and advances in analysis techniques since the dam was last analyzed in 1977. That investigation was part of a

¹ URS Corporation, Los Angeles, CA, USA

² Los Angeles Department of Water and Power, Los Angeles, CA, USA

broad California program of re-assessing the seismic stability of earth dams following the near failure of the Lower San Fernando dam in the 1971 San Fernando earthquake. Then, the dam was analyzed with the equivalent-linear finite-element program QUAD4 (Idriss et al. [1]). Due to this program's elasticity-based formulation, shaking-induced permanent deformations could not be computed directly. Instead, they were estimated by post-processing the QUAD4 results with the 'strain potential' procedure described by Lee [2], which computes gravity-induced slumping of the embankment as a result of soil softening due to cyclic loading. This procedure ignores inertial driving forces during shaking, which can accumulate large permanent deformations with a down-slope bias. In contrast, the plasticity-based, effective-stress approach used in this latest 2002 analysis not only takes into account these important driving forces, but also produces a more realistic dynamic response of the embankment by generating fully coupled pore pressures and associated strength loss during shaking. Going one step further, this investigation also included static and dynamic 3-D analyses of the dam, which were able to account for arching across the narrow alluvium-filled canyon at its base.

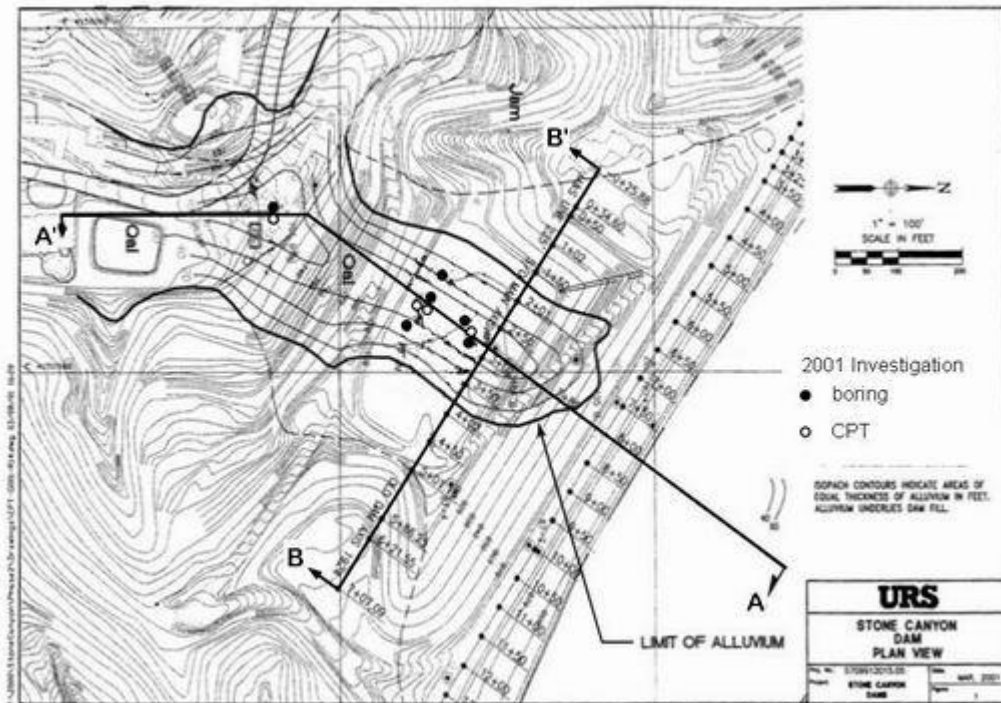


Figure 1. Stone Canyon Dam, Plan View with Contours of Alluvium Thickness

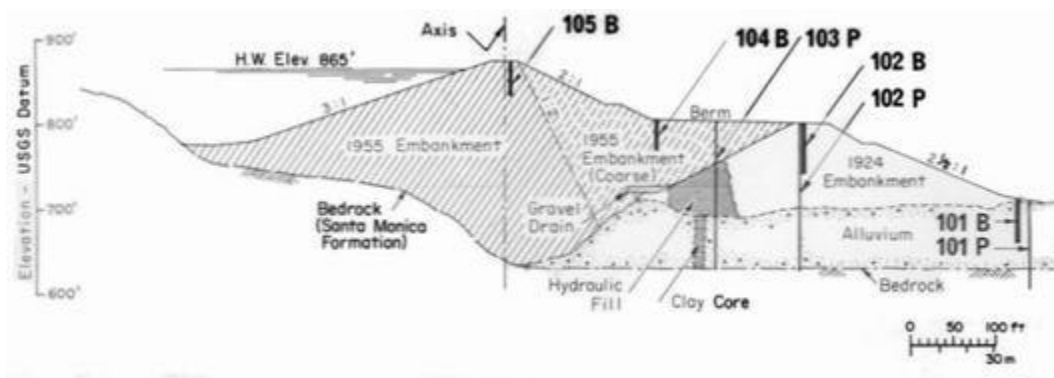


Figure 2. Cross Section A-A'

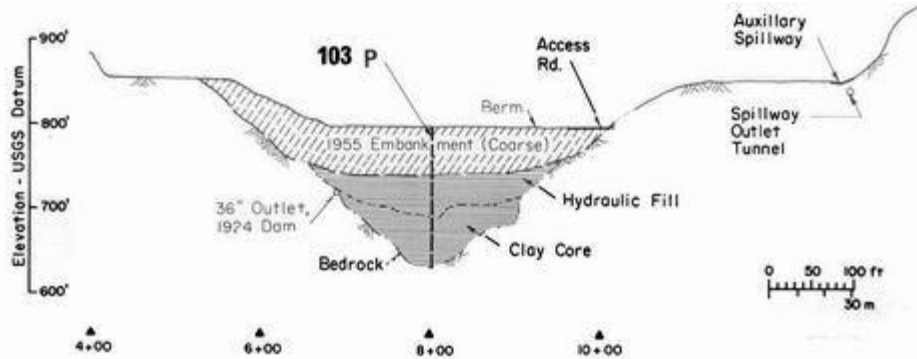


Figure 3. Transverse Section B-B'

GROUND MOTIONS

The dam was analyzed with 3 sets of acceleration time histories as described below.

1994 Northridge Earthquake

Acceleration histories from the 1994 Northridge earthquake were used for testing the dynamic-analysis approach by comparing computed and measured shaking-induced deformations. These histories were recorded at the dam site by strong-motion instruments deployed by the University of California Santa Barbara.

Regional MCE

An 84th percentile response spectrum for the regional Maximum Credible Earthquake (MCE) was derived by averaging spectra obtained from rock-site attenuation relationships by Abrahamson and Silva [3] and Sadigh, et al. [4]. Due to the scarcity of earthquake records available from large-magnitude events, a broadband ground motion history was generated for the Stone Canyon site. It represents a large earthquake involving the rupture of the Mojave and San Bernardino segments of the San Andreas faults, with the epicenter located southeast of Gorman. This history was then matched to the target spectrum for a magnitude $M_w=8$ earthquake.

Local MCE

A magnitude $M_w=6.5$ earthquake occurring on the Hollywood fault was considered as potential source for the local MCE. The fault is located only 3 km from the dam, and the style of faulting is oblique, with components of left-lateral strike-slip and north-dipping reverse slip. The dam is on the hanging wall of the fault, but at this close distance the effect is negligible (Abrahamson and Somerville [5]). First, separate strike-slip and reverse-slip earthquake response spectra were developed by averaging empirical rock-site attenuation models, as described above, and applying the near-fault directivity model of Somerville et al. [6]. The MCE spectrum shown in Figure 4 was then obtained by averaging these spectra.

In lieu of existing close-distance recordings from magnitude $M_w=6.5$ earthquakes with rupture mechanisms similar to the Hollywood fault, records of somewhat larger magnitude earthquakes were used for matching the MCE spectrum above. To compensate for this conservatism, recordings with relatively short durations were chosen as follows:

- (1) Erzincan recording of the 1992 Erzincan earthquake;
- (2) Los Angeles Dam recording of the 1994 Northridge earthquake; and
- (3) Lexington Dam recording of 1989 Loma Prieta earthquake.

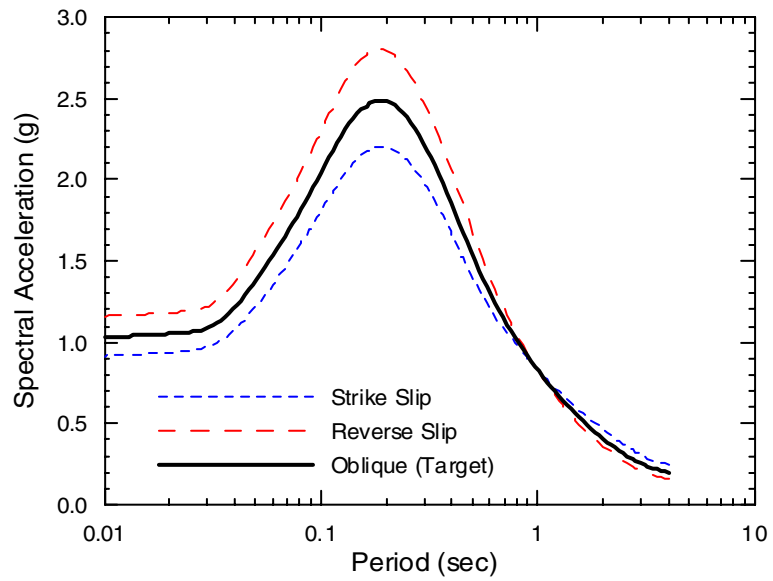


Figure 4. Target Response Spectrum for Local MCE

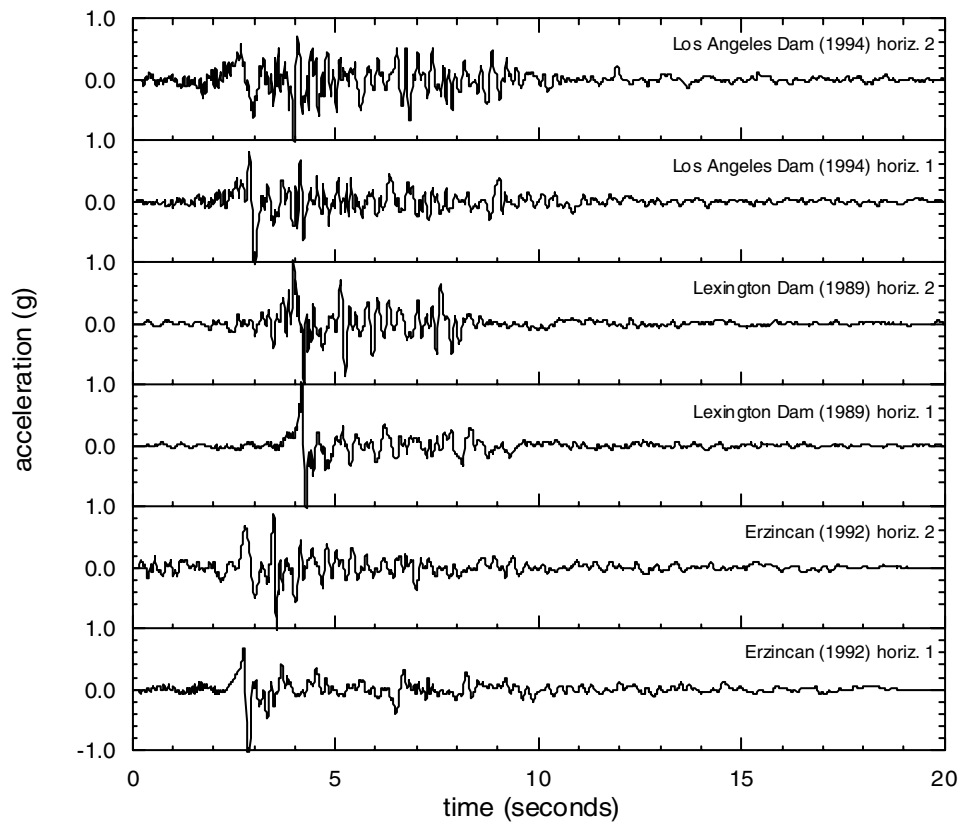


Figure 5. Acceleration Histories Matched to Target Spectrum for Local MCE

All of these records contain strong forward-rupture directivity effects. Their horizontal components were rotated to 45 degrees from fault normal, simulating the conditions at the Stone Canyon Dam site. The matched time histories resulting from these records are shown in Figure 5.

Deconvolved Motions

The outcrop motions above were deconvolved with SHAKE (Idriss et al. [7]) to derive the ‘within’ input motions to be applied at the base of the FLAC model. For this purpose, a soil column through the 1956 dam was analyzed using damping ratios of 5% and 2% for embankment materials and bedrock, respectively.

EMBANKMENT GEOMETRY AND MATERIAL PROPERTIES

At the outset of this study, a 2-D analysis of Stone Canyon Dam was performed for the maximum cross section shown in Figure 6. Detailed results of this analysis are presented in Zhai et al. [8]. The section analyzed (A-A' in Figure 1) runs along the bottom of the alluvial canyon, following its 30-degree turn at the downstream toe of the dam. Since the plane-strain analysis of this 2-D model neglects both arching across the narrow canyon, as well as the buttressing effect afforded by the turning of the canyon, the dam was also analyzed in 3-D.

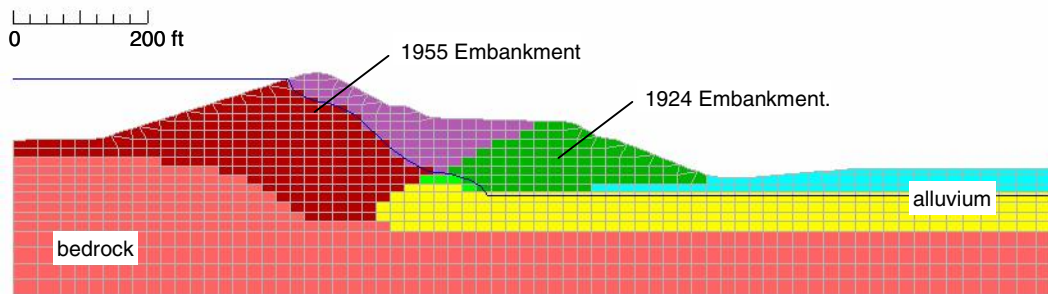


Figure 6. Numerical Mesh for 2-D Analysis (Section A-A')

Shear Strength and Elastic Modulus

The material properties of the embankment materials had been well defined in previous investigations (LADWP, [9]). Hence, additional field explorations for this study mainly focused on the alluvium underlying the downstream portion of the dam. Both SPT blow counts and CPT data were utilized for deriving shear-strength parameters, while shear moduli were derived from shear-wave velocities obtained with a Seismic Cone. The locations of the new (2001) borings and CPT soundings are shown in Figure 1, and the material properties are summarized in Table 1 below.

As shown in Figure 7, friction angles of 38 and 33 degrees were estimated for the 1924 embankment and underlying alluvium, respectively, from CPT data using relationships after Robertson et al. [10]. The shear moduli listed in Table 1 (from LADWP [9]), were found to be in good agreement with the shear-wave velocities measured in the alluvium, which ranged from 700 to 2,000 fps, with an average of 1,150 fps. The shear modulus for the bedrock material was estimated based on site-specific shear-wave velocity data obtained from the ROSRINE project (Resolution Of Site Response Issues from the Northridge Earthquake [11]), a government-academia-industry collaborative effort aimed at improving engineering models of earthquake ground motions.

Table 1. Soil Properties Used for Dynamic Analysis

Material	Unit Weight (pcf)	Shear Strength		Residual Shear Strength (psf)	Shear Modulus	
		Friction Angle (deg.)	Cohesion (psf)		K ⁽¹⁾	n ⁽¹⁾
1955 Embankment (unsaturated)	139	36	204		1056	0.493
1955 Embankment (saturated)	142	36	204	800	1056	0.493
1924 Embankment (unsaturated)	139	38	204		580	0.71
1924 Embankment (saturated)	142	38	204	800	580	0.71
Alluvium (unsaturated)	119	33	266		580	0.71
Alluvium (saturated)	132	33	266	800	580	0.71
Bedrock	142	-	-	-	45,000 ksf	
Notes: (1) $G = K P_a (\sigma'_m/P_a)^n$ where P_a is atmospheric pressure and σ'_m is mean effective stress						

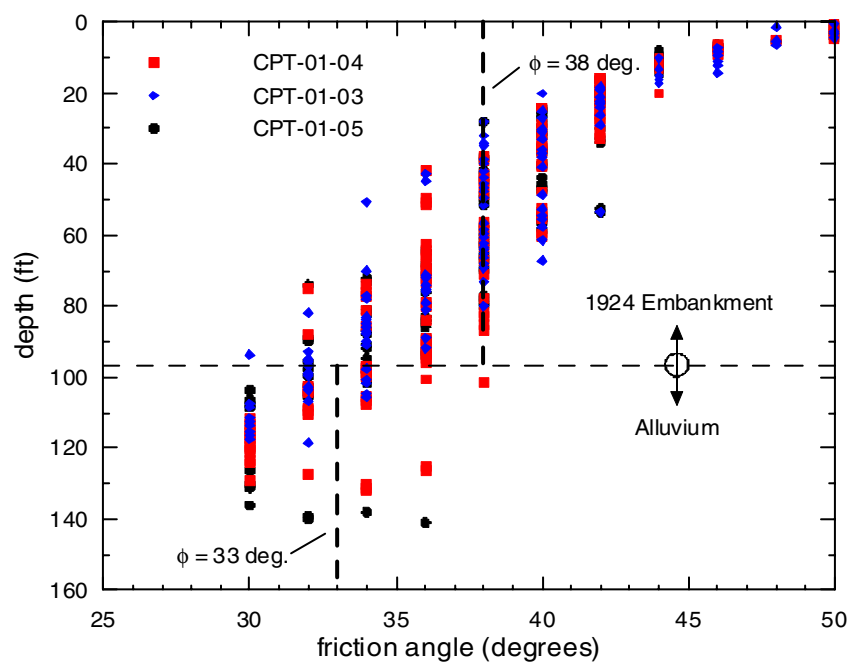


Figure 7. Friction Angles Estimated from CPT Data

Cyclic Shear Strength

The cyclic shear strength for alluvium was derived from equivalent clean-sand blow counts (Figure 8), based on relationships after Seed and coworkers (Seed et al. [12] and Seed [13]) as described by Dawson et al. [14]. After discarding blow counts greater than 30 as outliers, the mean of $(N_1)_{60\text{cs}}=19$ was considered to represent a best-estimate value for this purpose. In addition, a lower-bound value of $(N_1)_{60\text{cs}}=15$ was also established after removing all blow counts from samples containing large-size slate fragments, which may have biased the blow counts on the high side.

For the embankment fill, the cyclic strength was derived from previous (LADWP [9]) cyclic-triaxial tests on remolded samples of blended fill materials at a confining pressure of 2,000 psf. Curves for higher confining pressures were obtained using correction factors, K_σ , proposed by Youd and Idriss [15]. The cyclic-strength curves for both alluvium and embankment are shown in Figure 9.

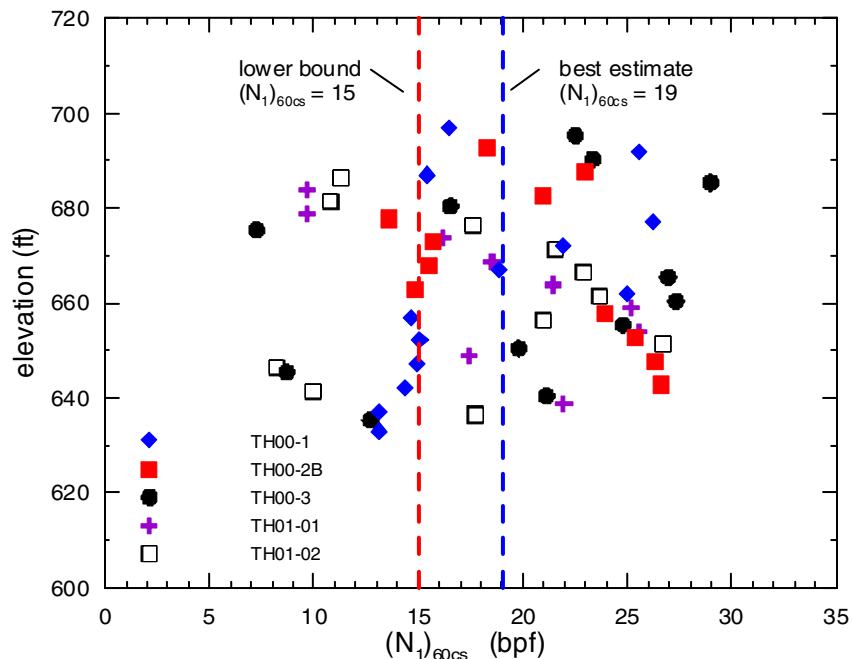


Figure 8. Equivalent Clean-Sand SPT Blow Counts of Alluvium

Residual Shear Strength

Post-liquefaction residual strengths for the saturated embankment and alluvium were derived from SPT blow counts from charts developed by Seed and Harder [16]. These charts are based on fines-corrections different from those used in deriving the cyclic-strength curves discussed above. Hence, to be consistent, a new set of equivalent clean-sand blow counts, $(N_1)_{60\text{cs}}$, was derived after Seed and Harder [16] for the purpose of estimating residual strength. With these new best-estimate and lower-bound $(N_1)_{60\text{cs}}$ values of 16 and 12, residual shear strengths of 800 psf and 400 psf, respectively, were obtained for the alluvium. The residual strength for the embankment was assigned to be 800 psf for all analysis runs.

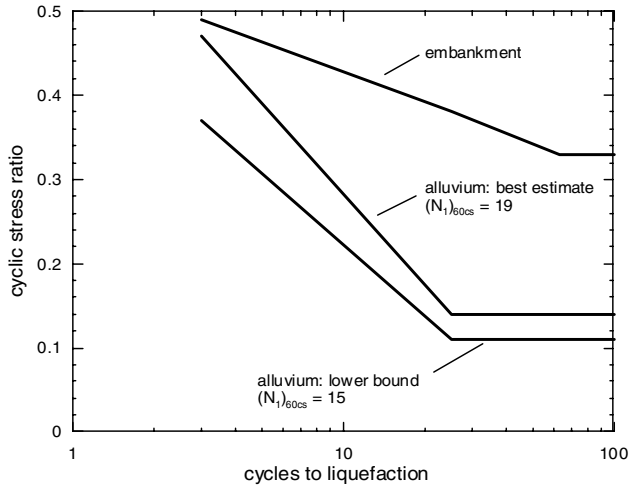


Figure 9. Cyclic Strength of Alluvium and Embankment

Damping

Damping in soils is primarily hysteretic, with energy dissipating when grains slide over one another. In the Mohr-Coulomb model, energy is dissipated by shaking-induced plastic flow when shear stresses reach the yield strength. For smaller stress cycles in the elastic range, energy dissipation is achieved by means of two viscous elements. Stiffness damping, as a function of strain rate, increases linearly with frequency; and mass damping, as a function of particle velocity, decreases exponentially with increasing frequency. By choosing a center frequency, at which the combined gradients of these two curves balance out, damping becomes nearly independent of frequency over a fairly wide spectrum. The center frequency is usually chosen in the range between the natural frequency of the model and the predominant frequency of the input motion.

Elastic-range damping ratios were assigned for each element of the dam model based on expected elastic shear-strain amplitudes for a given earthquake. Magnitudes of strain amplitudes were estimated by performing a linear-elastic analysis run before the actual nonlinear, effective-stress analysis. Damping ratios were taken for 65%-of-peak strain levels using relationships previously established from low-strain cyclic triaxial tests (LADWP [9]). Damping ratios obtained with this procedure ranged from 2% to 9% for the embankment and alluvium. For bedrock, 2% critical damping was utilized uniformly.

TWO-DIMENSIONAL DYNAMIC ANALYSES

Method of Analysis

Dynamic and 2-D post-shaking slope-stability analyses were performed with FLAC (Itasca [17]), an explicit finite difference program widely utilized for solving a broad range of problems in geomechanics, including nonlinear soil-structure interaction and groundwater flow. For this study, a Mohr-Coulomb (linear elastic/perfectly plastic) soil model was used, fully coupled with an empirical pore-pressure generation scheme. Pore pressures are updated every half shear-stress cycle, with an incremental version of the cyclic-stress approach developed by Seed and co-workers (Seed et al. [12] and Seed [13]). This incremental scheme was first introduced in 1985 for the dynamic analysis of Pleasant Valley dam (Roth et al [18]). Unlike the standard approach, where liquefaction potential is assessed as a post-processing step to equivalent-linear analysis, pore-pressure generation in FLAC is incremental and fully integrated with the nonlinear dynamic analysis. As effective stresses decrease with increasing pore water pressure, the soil begins to yield and increments of permanent deformation are accumulated during shaking.

The simultaneous coupling of pore-pressure generation with nonlinear, plasticity based, stress analysis produces a more realistic dynamic response than can be achieved with equivalent-linear methods. Specifically, the plastic strains generated as a result of increased pore pressures significantly contribute to internal damping of the modeled earth structure. This analysis approach has been verified by analyzing well documented seismic-performance case histories of dams (Roth et al. [19] and Bureau et al. [20]), as well as performing Type-A predictions of centrifuge shaking tests as part of NSF's VELACS program (Roth & Inel [21] and Inel et al. [22]). A detailed discussion of the dynamic pore-pressure generation scheme can be found in Dawson et.al. [14].

Test Run with 1994 Northridge Earthquake

At the outset, the dam model shown in Figure 6 was tested with input motions derived from the 1994 Northridge-earthquake recordings described earlier in this paper. The computed shaking-induced permanent deformations of up to 2 inches were somewhat greater than measured in the field, but of the same order of magnitude.

Regional-MCE Performance

Shaking the dam model with the Regional MCE produced horizontal and vertical permanent displacements of 1 and 2 inches, respectively, and some localized sloughing near the upstream toe of the dam. As such, shaking-induced deformations were significantly smaller than those resulting from Local-MCE shaking discussed below.

Local-MCE Performance

The 2-D model was analyzed for all six local-MCE motions shown in Figure 5, with the largest crest settlement computed for the *Erzincan H-2* input motion (Figure 10). Contours of excess-pore pressure ratios at the end of shaking, analyzed with best-estimate cyclic shear strength, are presented in Figure 11.

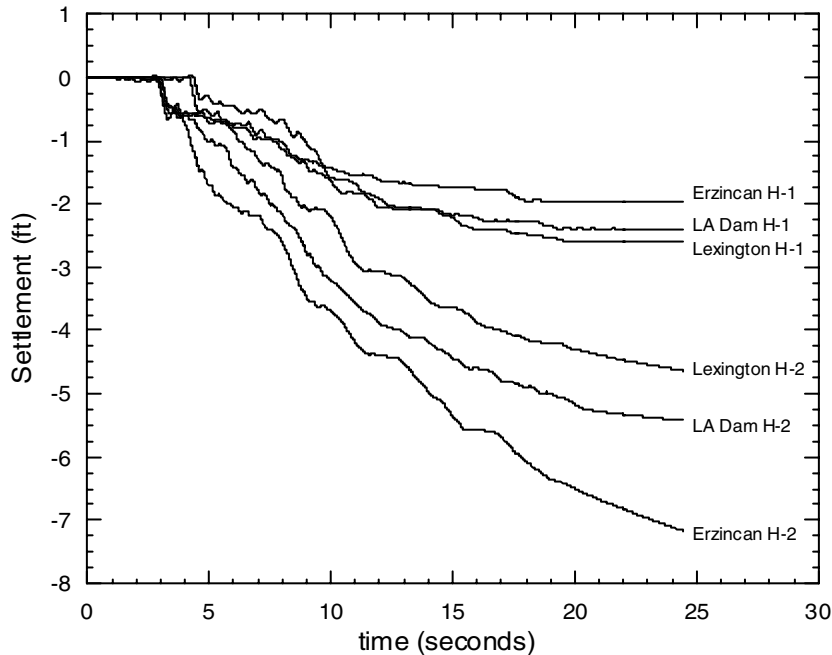


Figure 10. Crest Settlement Histories computed with 2-D Analyses; with Best-Estimate Cyclic Strength

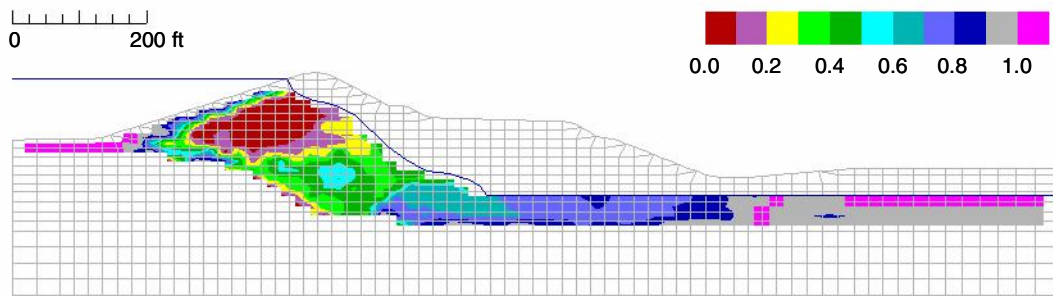


Figure 11. Excess Pore-Pressure Ratio at End of Shaking (2-D Analysis with Erzincan H-2 Motion)

As demonstrated by Mejia [23], a 2-D analysis of the maximum-height cross section of a short dam across a narrow canyon significantly underestimates its stability. In the case of Stone Canyon dam, its stability is greatly enhanced by the following conditions which can only be taken into account with a 3-D analysis:

- (1) Arching across the narrow canyon; and
- (2) Buttressing effect due to the turning of the alluvium canyon at the downstream toe.

Hence, it was decided to re-evaluate shaking-induced deformations and post-shaking stability in three dimensions, while using the results of the 2-D analysis merely to obtain a conservative estimate of shaking-induced excess pore pressures.

THREE-DIMENSIONAL ANALYSES

The 3-D model mesh of the dam is shown in Figure 12. The model was constructed from series of nine 2-D cross sections based on exploratory borings and dam-construction records. Hydrostatic pressure from the reservoir was taken into account by applying a pressure boundary condition on the upstream face of the dam.

Shear-Strength Reduction Technique

Post-shaking slope stability was analyzed with FLAC^{3D} [24] using the shear strength-reduction technique (Matsui & San [25]). In this procedure, the soil shear strength is reduced in stages until slope failure occurs, and the factor of safety is defined as the ratio of the soil's actual shear strength to the reduced strength at failure. Dawson et al. [26] demonstrated that this definition of a safety factor is identical to that used in conventional limit-equilibrium analyses with trial slip circles or failure planes.

The shear-strength reduction technique, combined with a continuum model, has a number of advantages over conventional analysis methods - especially for 3-D problems, or where non-isotropic soils, or embedded structural elements, are involved. As the shear strength is lowered, the only physically possible failure mode develops "naturally" without having to guess at trial failure configurations in advance. Hence, failures are not restricted to occur along circles, simple ellipsoids of revolution, or log-spirals, and they can also develop in the form of broad shear zones, rather than being forced on a distinct plane. The accuracy of the strength-reduction technique, using FLAC^{2D} and FLAC^{3D}, has been demonstrated through detailed comparisons with limit-equilibrium methods and closed-form solutions for simple homogeneous slopes (Dawson et al. [26, 27, 28] and Dawson and Roth [29]).

Post-Shaking Slope Stability

For the post-shaking stability analysis, pore pressures within the embankment portion of the 3-D model were imported from the 2-D model (after shaking it with the *Erzincan H-2* acceleration history) by projecting them perpendicular to the centerline of the canyon assuming uniform pore-pressure distribution between the canyon walls. Safety factors were computed for the full operating reservoir elevation of +865 ft.

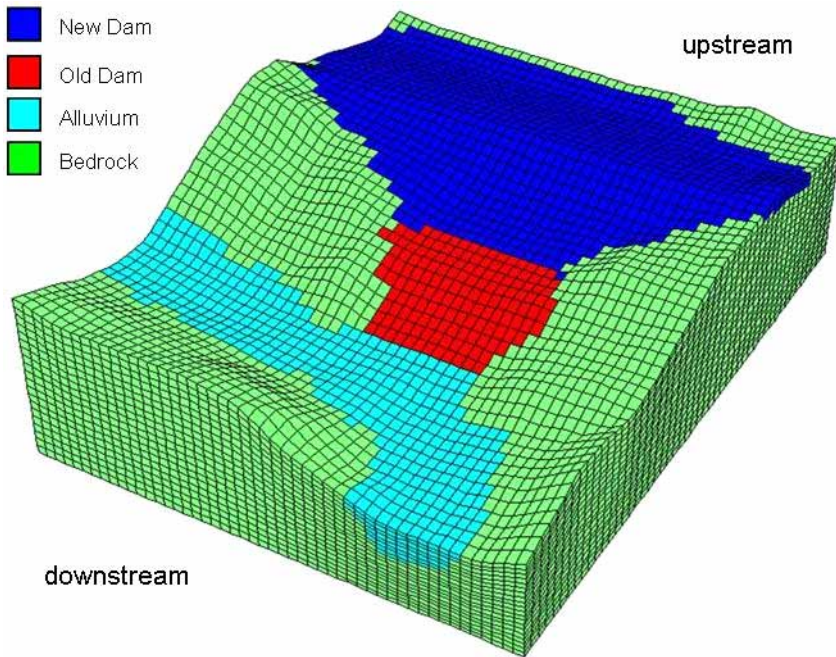


Figure 12. Numerical Mesh for 3-D Analysis

A slope-stability factor of safety of 1.6 was computed for the 3-D model with the post-shaking state based on the best-estimate cyclic strength for the alluvium. In Figures 13 and 14, the potential failure mode is illustrated with contours of velocity magnitudes at the onset of slope instability. This failure would be limited to the downstream berm without jeopardizing the stability of the upper, 1956 portion of the embankment which supports the crest of the dam. When re-analyzed with the assumption of lower-bound cyclic strength for the alluvium, the post-shaking safety factor decreased to 1.3, but the extent of the failure mode still did not impact the upper dam. Hence, the post-shaking safety factor against overtopping of the dam crest is even greater than 1.3.

Shaking-Induced Deformations

Shaking-induced permanent deformations were also analyzed with the 3-D model. Rather than generating excess pore pressures during shaking, the 3-D model was fully “charged” from the start with porepressures generated in the 2-D analysis discussed above. The input motion was then applied in the upstream-downstream direction, while the model was free to vibrate in both longitudinal and vertical directions.

The results for the analysis case with the best-estimate cyclic strength for the alluvium are shown in Figure 15. The center of the 1956 dam crest settled approximately 1 foot, while the downstream berm experienced localized sloughing with a 2-foot vertical drop. When repeating this analysis with the lower-bound cyclic strength for the alluvium, sloughing within the downstream berm increased, but the maximum crest settlement remained only about 1 foot. Because limited sloughing of the berm would not

endanger the overall stability of the embankment, it was concluded that the dam has a large margin of safety against overtopping during the worst-case local-MCE shaking scenario.

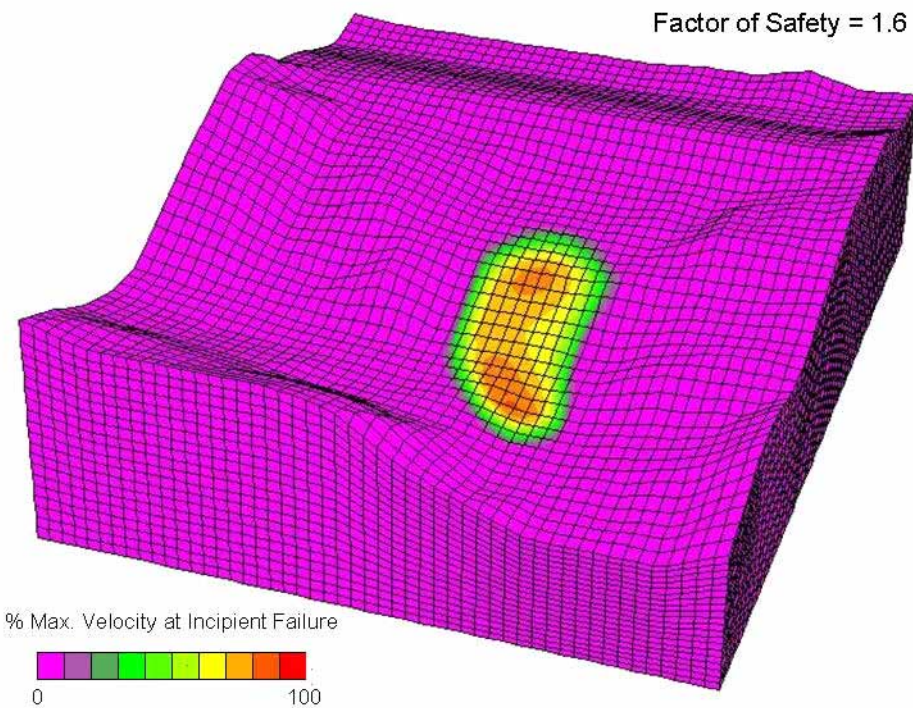


Figure 13. Post-Shaking Stability Analysis: Critical Failure Mode

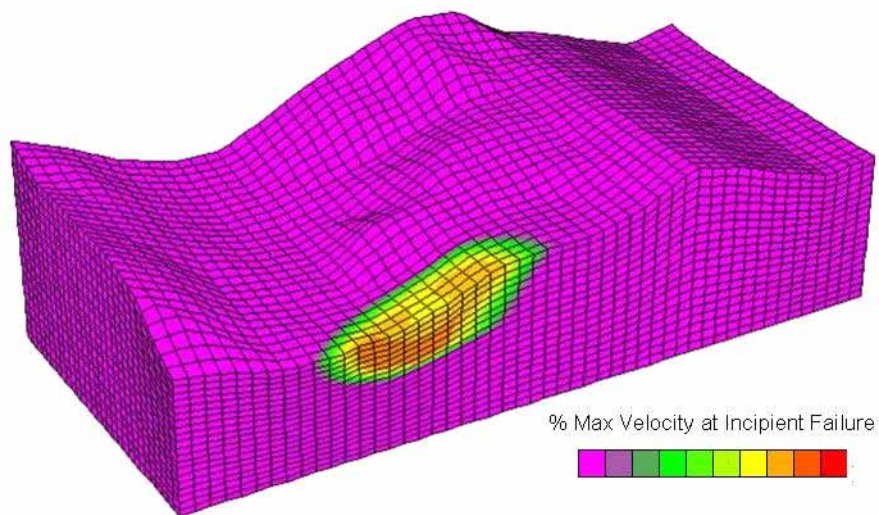


Figure 14. Post-Shaking Stability Analysis: Cut-Away View of Critical Failure Mode

CONCLUSIONS

The seismic performance of Lower Stone Canyon Dam was evaluated with 2-D and 3-D versions of the explicit finite-difference program FLAC utilizing an elastic-plastic Mohr-Coulomb soil model with effective stresses. The dam had been analyzed in 1977 with the equivalent-linear finite-element program QUAD4. Then, shaking-induced deformations were estimated without taking into account inertial forces which tend to accumulate permanent displacements with a down-slope bias. In contrast, the plasticity-based, effective-stress approach used in this latest 2002 analysis not only considers these inertial forces, but also produces a more realistic dynamic response of the embankment. Moreover, expanding the analysis to 3-D modeling allowed for a realistic assessment of arching across the narrow alluvium-filled canyon at the base of the dam. A comparison of 2-D versus 3-D analysis results highlights the inherent conservatism of evaluating the seismic stability of short dams across narrow canyons with 2-D plane-strain models.

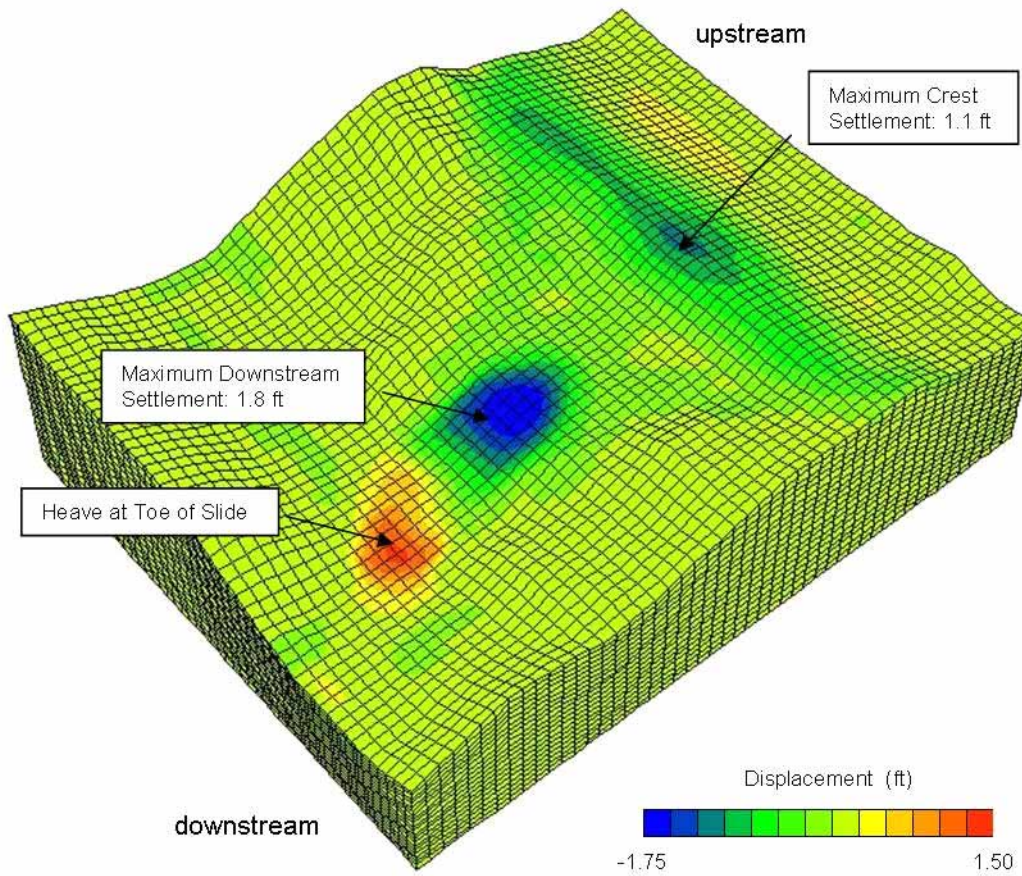


Figure 15. Shaking-Induced Settlement

For the governing local MCE the shaking-induced crest settlement was estimated to be about 1 foot, and would be accompanied by localized slumps in the downstream berm dropping about 2 feet. At the end of shaking, and without taking into account any pore-pressure dissipation, the slope-stability safety factor of the dam was estimated to range from 1.3 to 1.6 for lower-bound and best-estimate assumptions, respectively, of cyclic shear strength for the alluvium at the base of the dam. Based on these analysis results it was concluded that Lower Stone Canyon Dam can be operated safely with the reservoir level at its design elevation of 865 feet.

ACKNOWLEDGEMENTS

The work presented in this paper was commissioned by the Los Angeles Department of Water & Power. The authors wish to thank the Department, and especially Mr. George Brodt, for the encouragement and help provided for publishing this paper.

REFERENCES

1. Idriss, I.M., Lysmer, J., Hwang, R., and Seed, H.B. (1973). Quad-4, A Computer Program for Evaluating the Seismic Response of Soil Structures by Variable Damping Finite Element Procedures, Department of Civil Engineering, University of California, Berkeley, EERC 73-16, July.
2. Lee, K.L. (1975). Earthquake Induced Permanent Deformations of Embankments, Mechanics and Structures Department, School of Engineering and Applied Sciences, University of California, Los Angles, California, No. UCLA-ENG-7498, January.
3. Abrahamson, N.A. and Silva, W.J. (1997). Empirical Response Spectral Attenuation Relations for Shallow Crustal Earthquakes. *Seismological Research Letters*, Vol. 68, No. 1, pp. 94-127.
4. Sadigh, K., C.-Y. Chang, J.A. Egan, F. Makdisi, and R.R. Youngs 1997. Attenuation Relationships for Shallow Crustal Earthquakes Based on California Strong Motion Data, *Seismological Research Letters*, Vol. 68, No. 1, pp. 180-189.
5. Abrahamson, N.A. and P.G. Somerville (1996). Effects of the hanging wall and footwall on ground motions recorded during the Northridge Earthquake, *Bull. Seism. Soc. Am.*, 86, S93-S99.
6. Somerville, P.G., Smith, N.F., Graves, R.W. and Abrahamson, N.A. (1997). Modification of Empirical Strong Ground Motion Attenuation Relations to Include the Amplitude and Duration Effects of Rupture Directivity. *Seismological Res. Letters*, Vol. 68, No. 1, January/February 1997, pp. 199-222.
7. Idriss, I.M and Sun, J.I. (1992). SHAKE91: a computer program for conducting equivalent linear seismic response analyses of horizontally layered soil Deposits, Users Guide, University of California, Davis.
8. Zhai, E., Roth, W., Dawson, E., Davis, C. (1994). Seismic deformation analysis of an earth dam – a comparison study between equivalent-linear and nonlinear effective-stress approaches. Proceedings, 13th World Conference on Earthquake Engineering, Vancouver.
9. Los Angeles Department of Water and Power (LADWP), Dams Analysis Group, 1977. Stone Canyon Dam Stability Evaluation, March.
10. Robertson, P.K., Campanella, R.G. and Wightman, A. (1983). SPT-CPT correlations, *Journal of the Geotechnical Division of ASCE*, 109: 1449-1459.
11. ROSRINE project: Resolution of Site Response Issues from the Northridge Earthquake, 1998.
12. Seed, H.B., Martin, P.P., and Lysmer, J. (1976). Pore-Water Pressure Changes During Soil Liquefaction. *Journal of the Geotechnical Engineering Division, ASCE* , Vol. 102, No. GT4, pp 323-346.
13. Seed, H.B. (1979). Soil liquefaction and cyclic mobility evaluation for level ground during earthquakes. *Journal of the Geotechnical Engineering Division, ASCE*, Vol. 105 No. GT2, pp 201-255.
14. Dawson, E.M., Roth, W.H., Nesarajah, S., Bureau, G. and Davis, C.A. (2001). A Practice-Oriented Pore Pressure Generation Model. Proceedings 2nd International FLAC Symposium, Lyons, France, October.
15. Youd, T.L. and Idriss I.M. (2001). Liquefaction Resistance of Soils: Summary Report from the 1996 NCEER and 1998 NCEER/NSF Workshops on Evaluation of Liquefaction Resistance of Soils, *Journal of the Geotechnical and Geoenvironmental engineering, ASCE*, Vol. 127, No. 4, pp 297-313

16. Seed, H. B., Harder, L.F. (1990). SPT-based analysis of cyclic pore pressure generation and undrained residual strength. Proceedings of H.B. Seed Memorial Symposium, University of California, Berkeley, Vol. 2, pp. 351-376.
17. Itasca Consulting Group (2001). FLAC, Fast Lagrangian Analysis of Continua, Version 4.0. Itasca Consulting Group, Minneapolis, Minnesota, USA.
18. Roth, W.H., Bureau, G., and Brodt, G. (1991). Pleasant Valley Dam: An Approach to Quantifying the Effect of Foundation Liquefaction, 17th International Congress on Large Dams, Vienna.
19. Roth, W.H., Inel, S., Davis, C., and Brodt, G. (1993). Upper San Fernando Dam 1971 Revisited, 10th Annual Conference of the Association of State Dam Safety Officials, Kansas City, Missouri.
20. Bureau, G., Inel, S., Davis, C. A., and Roth, W.H. (1996), Seismic Response of Los Angeles Dam, California, During the 1994 Northridge Earthquake, USCOLD 1996 Annual Meeting and Lecture, Los Angeles, CA.
21. Roth, W.H., and Inel, S. (1993). An Engineering Approach to the Analysis of VELACS Centrifuge Tests, International Conference on the Verification of Numerical Procedures for the Analysis of Soil Liquefaction Problems, Davis, California. Arulanandan & Scott (eds.), Balkema, Rotterdam , pp 1209-1216.
22. Inel, S., Roth, W.H., and de Rubertis, C. (1993). Nonlinear Dynamic Effective-Stress Analysis of Two Case Histories, 3rd Int. Conf. on Case Histories in Geotechnical Engineering, St. Louis, Missouri. Paper No. 14.14, pp 1735-1741.
23. Mejia, L.H. (1989). Three-dimensional stability of an old dam, Proceedings of the 12th International Conference on Soil Mechanics and Foundation Engineering, Rio de Janeiro, August, pp. 1579-1582.
24. Itasca Consulting Group (2002). FLAC^{3D}, Fast Lagrangian Analysis of Contina in 3 Dimensions, Users's Guide. Itasca Consulting Group, Minneapolis, Minnesota, USA.
25. Matsui, T. & San, K.C. (1992). Finite element slope stability analysis by shear strength reduction technique. Soils and Found. 32, No. 1, 59-70.
26. Dawson, E.M., Roth, W.H. & Drescher, A. (1999). Slope stability Analysis by strength reduction. Géotechnique 49, No. 6, 835-840.
27. Dawson, E.M., You, K.H. and Park. Y.J. (2000). Strength-reduction stability analysis of rock slopes using the Hoek-Brown failure criterion. Trends in Rock Mechanics, ASCE Geotechnical Special Publication No. 102, pp. 65-77.
28. Dawson, E.M., Motamed, F., Nesarajah, S. and Roth. W.H. (2000). Geotechnical stability analysis by strength reduction. Slope Stability 2000, Geotechnical Special Publication No. 102, pp. 99-113.
29. Dawson, E.M., and Roth, W.H. (1999). Slope Stability Analysis with FLAC. Proc. of the Int. FLAC Symp. On Numerical Modeling in Geomechanics, Minneapolis, Minnesota, 1999. Detournay and Hart (eds), Balkema, Rotterdam, pp. 3-9.